Journal of Materials Chemistry A

Accepted Manuscript

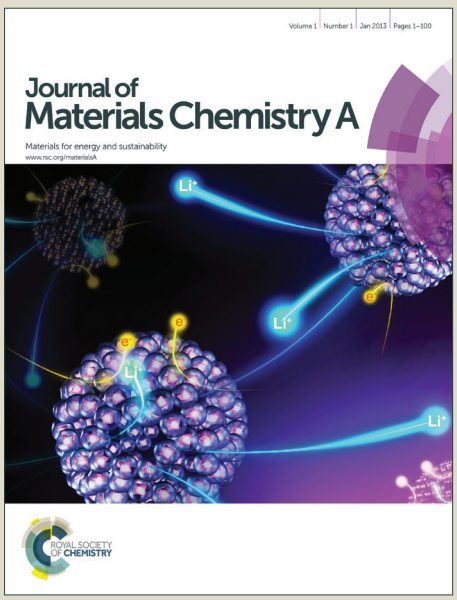

ROYAL SOCIETY OF CHEMISTRY

www.rsc.org/materialsA

Strontium Influence on the Oxygen Electrocatalysis of $La_{2-x}Sr_xNiO_{4\pm\delta}$ ($0.0 \leq x_{Sr} \leq 1.0$) Thin Films

Dongkyu Lee[1], Yueh-Lin Lee[1], Alexis Grimaud[1], Wesley T. Hong[1], Michael D. Biegalski[2], Dane Morgan[3] and Yang Shao-Horn[1,*]

[1]*Electrochemical Energy Laboratory, Massachusetts Institute of Technology, 77 Massachusetts Avenue, Cambridge, Massachusetts 02139, United States*

[2]*Center for Nanophase Materials Sciences, Oak Ridge National Laboratory, Oak Ridge, Tennessee 37831, United States*

[3]*Department of Materials Science and Engineering, University of Wisconsin–Madison, Madison, Wisconsin 53706, USA*

ABSTRACT

Substitution of lanthanum by strontium (Sr) on the A-site of cobalt-containing perovskites can greatly promote oxygen surface exchange kinetics at elevated temperatures. Little is known about the effect of A-site substitution on the oxygen electrocatalysis of Ruddlesden-Popper (RP) oxides. In this study, we report, for the first time, the growth and oxygen surface exchange kinetics of $La_{2-x}Sr_xNiO_{4\pm\delta}$ (LSNO, $0.0 \leq x_{Sr} \leq 1.0$) thin films grown on the $(001)_{cubic}$-Y_2O_3-stabilized ZrO_2 (YSZ) by pulsed laser deposition. High-resolution X-ray diffraction analysis revealed that the LSNO film orientation was changed gradually from the $(100)_{tetra.}$ (in-plane) to the $(001)_{tetra.}$ (out-of-plane) orientation in the RP structure with increasing Sr from $La_2NiO_{4+\delta}$ ($x_{Sr} = 0$) to $LaSrNiO_{4\pm\delta}$ ($x_{Sr} = 1.0$). Such a change in the LSNO film orientation was accompanied with reduction in the oxygen surface exchange kinetics by two orders of magnitude as shown from electrochemical impedance spectroscopy. Density function theory (DFT) calculations showed that Sr substitution could stabilize the $(001)_{tetra.}$ surface relative to the $(100)_{tetra.}$ surface and both Sr substitution and increasing $(001)_{tetra.}$ surface could greatly weaken adsorption of molecular oxygen on the La-La bridge sites in the RP structure, which can reduce oxygen surface exchange kinetics.

Keywords

Ruddlesden-Popper materials, solid oxide fuel cells, surface oxygen exchange kinetics, Sr substitution effect, crystallographic orientation effect, surface chemistry

Introduction

Perovskites (ABO_3) with high electronic and ionic conductivity and catalytic characteristics[1-3] have been studied intensively for solid oxide fuel cells (SOFCs)[1, 4-14] and oxygen permeation membranes[15] at high temperatures. A major barrier that limits the efficiency of SOFCs and oxygen permeation flux is the slow kinetics of oxygen surface exchange on the oxide surface. Mixed electronic and ionic conductors (MEICs) such as $La_{1-x}Sr_xCoO_{3-\delta}$ (LSC)[16-22] and $La_{1-x}Sr_xCo_{1-y}Fe_yO_{3-\delta}$ (LSCF)[23-26] are used commonly to promote the oxygen surface exchange kinetics, where the substitution of strontium (Sr) for lanthanum (La) in the A-site increases the surface exchange rates.[27, 28]

Ruddlesden-Popper (RP) oxides such as $La_2NiO_{4+\delta}$ (LNO) can lead to higher oxygen ionic conductivity relative to ABO_3 perovskites[29-32] and are interesting alternative cathode materials for SOFCs. The RP structure can be described as the intergrowth of alternative NiO_2 and La_2O_2 rock salt layers or layers of LNO separated by LaO layers (Fig. 1), having in-plane lattice parameters similar to that of perovskites in the pseudocubic notation. The oxygen stoichiometric La_2NiO_4 can be easily oxidized with additional interstitial oxygen incorporated into lanthanum tetrahedra in the La_2O_2 rock salt layer, which results in increasing the La-O bond distance and in decreasing the nickel ionic radius by the formation of Ni^{3+}.[33, 34] The alternating perovskite and rock salt layers in the RP structure can lead to different oxygen diffusion and surface exchange kinetics along different crystallographic directions. For example, the in-plane oxygen transport kinetics via interstitial oxygen diffusion in the LaO planes is considerably higher by up to two orders of magnitude compared to the out-of-plane kinetics[31] and the surface exchange kinetics in-plane can be an order of magnitude greater than that out-of-plane for LNO single crystals.[35] By substituting of a larger cation such as Sr^{2+} (1.31 Å) for La^{3+} (1.22 Å) in

LNO, the structural stresses are released, which leads to decrease in the amount of additional oxygen required to stabilize the structure and thus results in the reduction of the oxygen diffusion coefficients.[36, 37] However, the influence of Sr substitution on the in-plane and out-of-plane oxygen surface exchange kinetics of $La_{2-x}Sr_xNiO_{4\pm\delta}$ (LSNO) is poorly understood due to difficulties in the growth of single crystals of LSNO with high Sr substitution.[40]

Few studies have reported the oxygen surface exchange kinetics of polycrystalline LSNO with low Sr substitution (x_{Sr} = 0.1 and 0.2).[37-39] Skinner et al.[37] have shown no clear effect of the Sr substitution (x_{Sr} = 0.1) on the surface exchange kinetics whereas Boehm et al.[39] have reported that the Sr substitution (x_{Sr} = 0.1 and 0.2) can decrease the surface exchange kinetics. Synthesis of oriented RP films[41] grown on single-crystal substrates has enabled the studies of the oxygen surface exchange kinetics. For instance, employing out-of-plane-oriented LNO thin films grown on the $(001)_{cubic}$-$SrTiO_3$ (STO) and $(110)_{cubic}$-$NbGaO_3$ (NGO) substrates, Burriel et al.[31] have shown using secondary ion mass spectroscopy (SIMS) measurements that the in-plane oxygen surface exchange kinetics can be much greater than the out-of-plane kinetics, which is in agreement with measurements on single crystal LNO.[35] More recently, we have shown that the surface exchange coefficient, k^q, increases with increasing tensile volumetric strains and decreasing oxygen nonstoichiometry (δ) in LNO thin films.[42] Since the formation enthalpy of the oxygen interstitial has been shown to increase (less negative) with greater δ, the more negative oxygen interstitial formation enthalpy at lower δ suggests increase of the driving force to form interstitial oxygen in the RP structure. Therefore, the surface exchange kinetics of in-plane-oriented LNO thin films grown on $(001)_{cubic}$-Y_2O_3-stabilized ZrO_2 (YSZ) can be enhanced by increasing tensile volumetric strains.

In this study, we investigate how Sr substitution can affect the oxygen surface exchange

kinetics of LSNO thin films with a wide range of Sr content (x_{Sr} = 0.0, 0.2, 0.4, 0.6, 0.8, and 1.0) grown on YSZ. The surface orientation of these LSNO thin films (normal to the film surface) can be modified from the $(100)_{tetra.}$ (in-plane) to the $(001)_{tetra.}$ (out-of-plane) in the RP structure by increasing the Sr content from 0.0 to 1.0. Such a change in the film orientation can be explained by the reduction in the surface energy of the $(001)_{tetra.}$ surface with increasing Sr as revealed from Density function theory (DFT) calculations. Ex situ Auger electron spectroscopy (AES) indicates no formation of secondary phases across the Sr contents. We show a strong Sr dependence of the oxygen surface exchange rate (k^q) for the LSNO thin films, which can be attributed to the surface reorientation and the adsorption energy changes of molecular oxygen on the La-La bridge sites in the RP structure.

Experimental Methods

Film deposition

Pulsed laser deposition (PLD) was used to deposit the LSNO (x_{Sr} = 0.0, 0.2, 0.4, 0.6, 0.8, and 1.0) thin films on $(001)_{cubic}$-Y_2O_3-stabilized ZrO_2 (YSZ). A ~5 nm gadolinium-doped ceria (GDC, 20 mol % Gd) was also deposited between the LSNO and the YSZ as a buffer layer. Single crystal 9.5 mol% YSZ wafers with the $(001)_{cubic}$ orientation and dimensions of 10 × 5 × 0.5 mm (MTI corporation, USA) were used as the substrate. Prior to LSNO and GDC deposition, platinum ink (Pt) (#6082, BASF, USA) counter electrodes were painted on one side of the YSZ and dried at 900 ºC in air for 1 hour. The YSZ wafer was affixed to the PLD substrate holder using a small amount of silver paint (Leitsilber 200, Ted Pella, USA) for thermal contact. PLD was performed using a KrF excimer laser at λ = 248 nm, 10 Hz pulse rate and ~ 1.5 J/cm^2 pulse

energy under an oxygen partial pressure, $p(O_2)$ of 6.6×10^{-5} atm (50 mTorr) with 500 pulses of GDC (~5 nm) at 550 °C, followed by 5,000 pulses of LSNO (x_{Sr} = 0.0, 0.2, 0.4, 0.6, 0.8, and 1.0) at 650 ºC. The film thicknesses were determined by atomic force microscopy (AFM). Details of the thickness information are provided in the Electronic Supplementary Information (ESI). The utilization of reflection high-energy electron diffraction (RHEED) enabled an in-situ monitoring of the LSNO film growth. After completing the LSNO deposition, the samples were cooled down to room temperature in the PLD chamber for ~1 hour under a $p(O_2)$ of 6.6×10^{-5} atm (50 mTorr). The synthesis details of LSNO and GDC PLD targets can be found in the ESI.

High resolution X-ray diffraction (HRXRD)

The oxide phase purity and the thin film orientations were investigated via high-resolution X-ray diffraction (HRXRD) using a four-circle diffractometer (PANalytical, USA and Bruker D8, Germany). Measurements were performed in normal and off-normal configurations. The LSNO thin films showed a structural reorientation as a function of Sr content and the determination of in-plane $\boldsymbol{a}_{\text{tetra.}}$ and out-of-plane $\boldsymbol{c}_{\text{tetra.}}$ lattice parameters was described below, where the subscript "tetra." denotes the tetragonal notation. The LNO structure can be influenced greatly by the oxygen stoichiometry and fully oxidized $La_2NiO_{4.25}$ exhibits a monoclinic symmetry with space group C2 at room temperature[43] while stoichiometric La_2NiO_4 is orthorhombic with space group Bmab.[44] The LSNO oxides up to x_{Sr} = 1.0 are well known to have tetragonal symmetry with space group I4/mmm.[45, 46] However, the oxygen nonsotichiometry of the LNO thin film is experimentally challenging to obtain precisely, and the XRD data of single-crystalline thin films do not readily allow a precise refinement of the symmetry of the LNO structure. Therefore, the LNO film was considered to have tetragonal symmetry with space group I4/mmm, which differs

from the orthorhombic by the loss of the octahedral tilting (≤ 1°)[44] and the tetragonal symmetry is generally used to describe the system in thin film studies.[42] The in-plane $\boldsymbol{a}_{\text{tetra.}}$ parameter of LSNO normal to the film surface was determined from the $(200)_{\text{tetra.}}$ peak positions and the out-of-plane $\boldsymbol{c}_{\text{tetra.}}$ parameter of the LSNO thin films with x_{Sr} = 0 and 0.2 was determined from the off-normal $(103)_{\text{tetra.}}$ peak position. For the LSNO thin films with x_{Sr} = 0.4, 0.6, 0.8, and 1.0, the in-plane $\boldsymbol{a}_{\text{tetra.}}$ parameter and the out-of-plane $\boldsymbol{c}_{\text{tetra.}}$ parameter were determined from the off-normal $(103)_{\text{tetra.}}$, and $(006)_{\text{tetra.}}$ peak positions, respectively.

Atomic Force Microscopy (AFM)

The surface morphology was examined by optical microscopy (Carl Zeiss, Germany) and atomic force microscopy (AFM) (Veeco, USA). The RMS (root-mean-square) roughness value of LSNO with x_{Sr} = 0.0 and 1.0 was found to show about 0.3 nm while that of LSNO with x_{Sr} = 0.2, 0.4, 0.6, and 0.8 was found to show about 0.6 nm as shown in Fig. S5.

Electrochemical impedance spectroscopy (EIS)

In situ electrochemical impedance spectroscopy (EIS) measurements of LSNO microelectrodes ~200 μm in diameter were performed using a microprobe station (Karl Süss, Germany) connected to a frequency response analyzer (Solartron 1260, USA) and dielectric interface (Solartron 1296, USA). Temperature was controlled at 550 °C using a heating stage (Linkam TS1500, UK) and data were collected between 1 MHz to 1 mHz using a voltage amplitude of 10 mV. EIS testing temperature was calibrated with a thermocouple contacting the thin film surface and deviation of ± 5 °C was observed. EIS experiments were performed as a function of $p(O_2)$ between 10^{-3} and 1 atm. Multiple electrodes (at least three) of all films were measured by EIS at

each temperature and $p(O_2)$ to ensure that the EIS results were reproducible and representative. EIS data of all samples used in this study were found to show nearly perfect semicircle impedances,[1] and typical features in the Nyquist plots are shown in the schematic in Fig. S7c. EIS data were analyzed using an equivalent circuit (Fig. S7b), where the high-frequency intercept corresponds to the oxygen ion conduction resistance in YSZ and the mid-frequency feature is believed to result from the interface between YSZ and GDC as reported previously.[17, 19, 42]

Considering the fact that the film thicknesses are much smaller than the critical thickness, t_{crit}, defined as D^*/k^*, where D^* is the tracer oxygen diffusivity and k^* is the tracer surface exchange coefficient[47] (350 μm estimated for the LNO[35] and 888 μm estimated for LSNO having x_{Sr} = 0.2[39] at 550 °C), the $p(O_2)$-dependent impedance responses suggest that the oxygen surface exchange kinetics governs the oxygen electrocatalysis on the LSNO thin film surface. The surface exchange rate was calculated from the resistance of the low-frequency semicircle using[19, 42, 48, 49] $k^q = \frac{RT}{4F^2 R_{LF} A_{electrode} c_0}$, where R is the universal gas constant (8.314 J mol^{-1}·K^{-1}), T is the absolute temperature (823 K), F is the Faraday's constant (96,500 C·mol^{-1}), $A_{electrode}$ is the area of the microelectrode, and c_0 is the lattice oxygen concentration in LSNO. Details about the EIS testing procedure, data analysis, and c_0 estimation can be found in the ESI.

Ex situ Auger electron spectroscopy (AES)

Ex situ Auger electron spectroscopy (AES) was conducted to analyze the surface chemistry change of LSNO films after annealing on a Physical Electronics 700 Scanning Auger Nanoprobe (PHI, USA) operating at an accelerating voltage of 10 kV. The films were annealed at 550 °C for 6 hours in an oxygen partial pressure of 1 atm before AES data were collected. The

AES data were collected from three different areas (10 μm × 10 μm) selected on a sample in an ultra high vacuum chamber. Elemental quantification of AES spectra utilized relative sensitivity factors (RSFs) of 0.059, 0.027, 0.227, and 0.212 for La_{MNN}, Sr_{LMM}, Ni_{LMM}, and O_{KLL}, respectively, as supplied by the AES manufacturer (Physical Electronics).

Density Functional Theory (DFT)

Spin-polarized Density Functional Theory (DFT) calculations were preformed with the Vienna *Ab-initio* Simulation Package[50, 51] using the Projector-Augmented plane-Wave method[52] with a cutoff energy of 450 eV. Exchange-correlation was treated in the Perdew-Wang-91.[53] Generalized Gradient Approximation (GGA) using the soft O_s oxygen pseudopotential. The GGA+U calculations[54] were performed with the simplified spherically averaged approach,[55] where the U_{eff} (U_{eff} = Coulomb U - exchange J) is applied to d electrons (U_{eff}(Ni) = 6.4 eV). All calculations were performed in the ferromagnetic state in order to use a consistent and tractable set of magnetic structures, and the Ni cations are in the high spin state for x_{Sr} = 0.0 with even reduction on spin moment of each Ni cation when increasing Sr (hole) doping. Details about the calculation for bulk LSNO, surface energy and oxygen adsorption energy can be found in the ESI.

Results and discussion

Structural reorientation of the LSNO thin films with increasing Sr content

Normal HRXRD data in Fig. 2a clearly showed a structural reorientation of LSNO thin films as a function of Sr content (Fig. 2a). The LNO film (x_{Sr} = 0.0) was found to have the

$(l00)_{tetra.}$ (l is even) peaks only and the $(00l)_{cubic}$ (l is even) peaks of GDC and YSZ, which indicates that the LNO film grew epitaxially with the $\boldsymbol{a}_{tetra.}$-axis perpendicular to the film surface. With x_{Sr} in LSNO equal to and greater than 0.2, the films were found to exhibit not only $(l00)_{tetra.}$ (l is even) but also $(00l)_{tetra.}$ (l is even) peaks, indicating the presence of both domains with the $\boldsymbol{a}_{tetra.}$-axis and $\boldsymbol{c}_{tetra.}$-axis perpendicular to the film surface. The intensities of LSNO $(00l)_{tetra.}$ peaks were found to increase with increasing Sr content in LSNO while those of the $(l00)_{tetra.}$ peaks decreased, where the intensity ratio between the $(200)_{tetra.}$ and the $(006)_{tetra.}$ peaks of the LSNO thin films decreasing with increasing Sr is shown as an example in Fig. S3a. This observation suggests that Sr substitution of La in LSNO thin films promotes the $(00l)_{tetra.}$ orientation growth but suppresses the growth of the $(l00)_{tetra.}$ orientation. Only the $(00l)_{tetra.}$ (l is even) peaks were found for LSNO with $x_{Sr} = 1.0$, indicating that the film was single crystalline with the $\boldsymbol{c}_{tetra.}$-axis perpendicular to the film surface, as shown in Fig. 2a. Off-normal phi-scan analysis (Fig. 2c) allowed us to identify the in-plane crystallographic relationships among LSNO, GDC and YSZ. The $[100]_{tetra.}$ direction in the $\boldsymbol{a}_{tetra.}$-axis-oriented LSNO and the $[001]_{tetra.}$ direction in the $\boldsymbol{c}_{tetra.}$-axis-oriented LSNO were rotated by 45° with respect to the $[001]_{cubic}$ direction of GDC. Moreover, as expected from increasing Ni oxidation from Ni^{2+} in LNO to Ni^{3+} in LSNO, the $(l00)_{tetra.}$ and $(00l)_{tetra.}$ interplanar distances of LSNO were shifted towards higher diffraction angles with increasing Sr (Fig. S3b).

The relaxed lattice parameters $\hat{\boldsymbol{a}}_{tetra.}$ and $\hat{\boldsymbol{c}}_{tetra.}$ of LSNO thin films at room temperature were found to be in the range of 3.81 – 3.91 Å and 12.44 – 12.72 Å, respectively. Details of the lattice parameters are provided in the ESI. Interestingly, the relaxed lattice $\hat{\boldsymbol{a}}_{tetra.}$ parameter was found to decrease with the Sr content for $0.0 \leq x_{Sr} \leq 0.6$ while it slightly increased with increasing Sr for $x_{Sr} > 0.6$. In contrast, the relaxed lattice $\hat{\boldsymbol{c}}_{tetra.}$ parameter was found to exhibit the

opposite trend, which results in a maximum in the $\boldsymbol{c}_{tetra.}/\boldsymbol{a}_{tetra.}$ ratio (tetragonality) at $x_{Sr} = 0.6$, as shown in Fig. S1. As described for bulk LSNO,[46] the decrease of the in-plane parameters ($\boldsymbol{a}_{tetra.}$ and $\boldsymbol{b}_{tetra.}$) is due to the oxidation of nickel and the increase of the out-of-plane $\boldsymbol{c}_{tetra.}$ parameter is correlated with the replacement of La^{3+} by Sr^{2+}. For $x_{Sr} > 0.6$, the opposite trend is observed, which has been explained by Jahn-Teller distortion.[45]

The change in the orientation of LSNO films with increasing Sr can be explained by the difference in the surface energy of in-plane and out-of-plane atomic terminations in the RP structure.[41, 56, 57] As shown in Fig. 3a, the calculated surface energies (details of the DFT modeling are provided in the ESI) of LSNO $(100)_{tetra.}$ and $(001)_{tetra.}$ planes were found to be strongly dependent on the Sr content, where the surface energy of $(100)_{tetra.}$ plane was found to decrease while that of the $(001)_{tetra.}$ plane increased with increasing Sr content in LSNO.[57] It is interesting to note that the strain energies of the LSNO thin films were found to be significantly lower than the surface energy (Fig. 3a, details of strain energy calculation are provided in the ESI), which suggests that the strain energy in LSNO is not strongly correlated with the structure reorientation of LSNO thin films. Furthermore, the lattice mismatch between LSNO and GDC, YSZ was found to be independent of the Sr content (Table S1), which further suggests that the structure reorientation is not a result of the film strain. Therefore, the film reorientation can be attributed to the reduction of the surface energy of LSNO films.

Oxygen surface exchange kinetics of the LSNO thin films

EIS data collected from the LSNO thin films as a function of Sr at an oxygen partial pressure ($p(O_2)$) of 1 atm and T = 550 °C are shown in Fig. 4a. The real part of the impedance of the predominant semicircle increased significantly with increasing the Sr content of LSNO thin

films, from which the k^q values of LSNO were found to decrease with increasing the Sr content. In addition, the predominant semicircle was found to increase with decreasing $p(O_2)$ for all compositions, and representative EIS data collected from LSNO with x_{Sr} = 0.2 at 550 °C as a function of $p(O_2)$ are shown in Fig. 4b. Assuming that k^q can be approximated as k^*,[58] the k^q trend of the LSNO thin films is in good agreement with that of bulk LSNO with x_{Sr} = 0.1 and 0.2.[39] Representative k^q values of the LSNO thin films as a function of the Sr content obtained at $p(O_2)$ = 1 atm and T = 550 °C are shown in Fig. 5. The k^q values of the $\boldsymbol{a}_{tetra.}$-axis-oriented LNO (x_{Sr} = 0.0) are two orders of magnitude higher than that of the $\boldsymbol{c}_{tetra.}$-axis-oriented LSNO (x_{Sr} = 1.0), where the k^q values of the LSNO thin films decreased with increasing orientation having the $\boldsymbol{c}_{tetra.}$-axis perpendicular to the film surface with increasing Sr.

Proposed origin for the oxygen surface exchange kinetics of LSNO as a function of the Sr content

The volume specific capacitances (*VSCs*) extracted from EIS data of the LSNO thin films (details are provided in the ESI), corresponding to the change in the oxygen nonstoichiometry (δ) induced by the change in the electrical potential, are in good agreement with the δ trend of the bulk LSNO,[59] as shown in Fig. 4d. However, the *VSCs* of the LSNO thin films with $0.4 \leq x_{Sr} \leq 1.0$ were found to be independent on the $p(O_2)$, whereas the k^q values of the LSNO thin films were found to increase with increasing the $p(O_2)$ as expected (Fig. 4c). Previously, we reported that the δ of the LSC thin films might not control the oxygen surface exchange kinetics.[17] Moreover, it has been reported that the diffusion coefficients (D^*), which can be influenced by the oxygen content in the LNO thin films have no correlation with the surface exchange coefficients (k^*).[31] Therefore, the change in the oxygen content induced by the Sr content in the

LSNO thin films cannot contribute to the modification in the k^q values observed.

To investigate the change in the surface chemistry of the LSNO thin films as a function of the Sr content, ex situ AES was conducted on the LSNO thin films after annealing at 550 °C in an oxygen partial pressure of 1 atm. Fig. 6 shows the surface La_{MNN}, Sr_{LMM}, and Ni_{LMM} cations spectra of each film. The intensity of La cation spectra was found to decrease with increasing the Sr content (Fig. 6a), whereas the intensity of Sr cation spectra was found to increase (Fig. 6b), as expected from the nominal composition. This clearly indicates that the surface chemistry is representative of the surface cationic ratio targeted. It should be noted that the intensity of Ni cation spectra was found to increase with increasing the Sr content, as shown in Fig. 6c. In the case of $\boldsymbol{c}_{tetra.}$-axis-oriented LSNO thin film with x_{Sr} = 1.0, the $(001)_{tetra.}$ planes have more NiO_6 octahedra by surface area relative to the $(100)_{tetra.}$ planes. The relative sensitivity factor (RSF) of Ni (RSF: 0.277) is sensitively higher than that of La (RSF: 0.059) and Sr (RSF: 0.027). The intensity of Ni cation spectra can therefore be attributed to the thin film reorientation from the $(100)_{tetra.}$ to the $(001)_{tetra.}$ orientation, as observed by HRXRD. Furthermore, no spectral changes were observed for any of the cation Auger lines as a function of the Sr content, suggesting that no formation of secondary phases occurred across the range of Sr content. This was further confirmed by scanning electron microscopy (SEM) (Fig. S6), where the surface morphology of each film was found to be stable after annealing.

The surface exchange kinetics is highly anisotropic in the RP structure.[31, 56] Burriel et al.[31] have shown from secondary ion mass spectroscopy (SIMS) measurements that the oxygen surface exchange kinetics in the $(100)_{tetra.}$ plane is two orders of magnitude greater than that along the $(001)_{tetra.}$ plane in LNO thin films. The difference can be attributed to the fact that the exposed interstitial sites of the $(100)_{tetra.}$ surfaces provide active sites for the oxygen surface

exchange and incorporation, whereas the $(001)_{tetra.}$ planes have no interstitial oxygen sites due to the perovskite layers, blocking interstitial site oxygen incorporation, as shown in Fig 1. Kim et al.[56] have also reported using electrical conductivity relaxation (ECR) measurement in LNO thin films that the surface exchange kinetics in the $(001)_{tetra.}$ plane is two orders of magnitude slower than that in the $(100)_{tetra.}$ plane, which also supports the influence of anisotropy on the surface exchange kinetics in the RP structure. Therefore, the decrease of the observed k^q values of the LSNO thin films as a function of the Sr content can be partly attributed to the orientation effect, as shown in Fig. 5.

Surface exchange kinetics of the RP structure can also be influenced by the oxygen adsorption energy.[60] The weaker adsorption (the less negative adsorption energy) was found to accompany with higher Sr content for LSNO, regardless of the anisotropy of oxygen adsorption, as shown in Fig. 3b. The weakening in the oxygen adsorption upon Sr substitution can be attributed to the increased oxidation state of the transition metal cations and the reduction of surface polarity (surface layer charge) induced with the Sr substitution, both of which certainly contribute to weaken the oxygen binding.[61] Consequently, the reduced oxygen adsorption caused by the Sr substitution may provide a reduced flux of oxygen for the oxygen incorporation kinetics, and can be another reason for the strong Sr content dependence of the surface exchange rate for the LSNO thin films, as shown in Fig. 5.

Although the oxygen surface exchange kinetics are not strongly correlated with the electrical conductivity in LNO thin films,[31, 62] the influence of hole concentration and mobility of Sr and Ni cations on the oxygen surface exchange kinetics cannot be excluded, and their role requires further investigation.

Conclusions

In summary, we have successfully deposited epitaxial LSNO thin films with different Sr content ($0.0 \leq x_{Sr} \leq 1.0$) by PLD. HRXRD reveals that the Sr substitution leads to a structural reorientation from the $(100)_{tetra.}$ (in-plane) to $(001)_{tetra.}$ (out-of-plane) orientation as a function of the Sr content, which is further supported by the DFT and AES analysis. The k^q value of the LSNO thin films is found to strongly depend on the Sr content: the k^q of the LSNO thin films decreases with increasing the Sr content. DFT modeling shows that the trend in adsorption energies of the LSNO system decreases oxygen surface binding with increasing Sr contents. Ex situ AES shows that there is no formation of second phases or phase segregation as a function of the Sr content. Our results demonstrate the key role of Sr substitution of RP phases on the oxygen surface exchange process, where modifying the orientation and the adsorption energy by Sr substitution is a new strategy to design oxygen surface exchange materials with desired anisotropic characteristics for applications such as SOFC cathodes or oxygen conducting membranes.

ASSOCIATED CONTENT

† Electronic supplementary information (ESI) available: Experimental details (target synthesis, PLD, micro-patterning, HRXRD) of PLD target materials, correlation of ‘‘Sr’’ film thickness after PLD deposition and the number of PLD laser pulses, information on the electrochemical testing and analysis, AFM, SEM, AES, and DFT details.

AUTHOR INFORMATION

Corresponding Author

* shaohorn@mit.edu

ACKNOWLEDGMENT

This work was supported in part by DOE (SISGR DESC0002633) and King Abdullah University of Science and Technology. The authors like to thank the King Fahd University of Petroleum and Minerals in Dharam, Saudi Arabia, for funding the research reported in this paper through the Center for Clean Water and Clean Energy at MIT and KFUPM. The PLD was conducted at the Center for Nanophase Materials Sciences, which is sponsored at Oak Ridge National Laboratory by the Scientific User Facilities Division, Office of Basic Energy Sciences, U.S. Department of Energy.

References

1. S. B. Adler, *Chem. Rev.*, 2004, **104**, 4791-4843.
2. A. S. Bhalla, R. Y. Guo and R. Roy, *Mater. Res. Innov.*, 2000, **4**, 3-26.
3. R. J. H. Voorhoeve, D. W. Johnson, J. P. Remeika and P. K. Gallagher, *Science*, 1977, **195**, 827-833.
4. S. B. Adler, X. Y. Chen and J. R. Wilson, *J. Catal.*, 2007, **245**, 91-109.
5. L. da Conceicao, C. R. B. Silva, N. F. P. Ribeiro and M. Souza, *Mater. Charact.*, 2009, **60**, 1417-1423.

6. R. A. De Souza and J. A. Kilner, *Solid State Ion.*, 1998, **106**, 175-187.

7. R. A. De Souza and J. A. Kilner, *Solid State Ion.*, 1999, **126**, 153-161.

8. P. Decorse, G. Caboche and L. C. Dufour, *Solid State Ion.*, 1999, **117**, 161-169.

9. T. Ioroi, T. Hara, Y. Uchimoto, Z. Ogumi and Z. Takehara, *J. Electrochem. Soc.*, 1997, **144**, 1362-1370.

10. A. J. Jacobson, *Chem. Mat.*, 2010, **22**, 660-674.

11. Y. L. Lee, J. Kleis, J. Rossmeisl and D. Morgan, *Phys. Rev. B*, 2009, **80**.

12. Z. P. Shao and S. M. Haile, *Nature*, 2004, **431**, 170-173.

13. B. C. H. Steele and A. Heinzel, *Nature*, 2001, **414**, 345-352.

14. C. W. Sun, R. Hui and J. Roller, *J. Solid State Electrochem.*, 2010, **14**, 1125-1144.

15. S. M. Hashim, A. R. Mohamed and S. Bhatia, *Adv. Colloid Interface Sci.*, 2010, **160**, 88-100.

16. S. B. Adler, *Solid State Ion.*, 1998, **111**, 125-134.

17. E. J. Crumlin, S. J. Ahn, D. Lee, E. Mutoro, M. D. Biegalski, H. M. Christen and Y. Shao-Horn, *J. Electrochem. Soc.*, 2012, **159**, F219-F225.

18. E. J. Crumlin, E. Mutoro, Z. Liu, M. E. Grass, M. D. Biegalski, Y. L. Lee, D. Morgan, H. M. Christen, H. Bluhm and Y. Shao-Horn, *Energy Environ. Sci.*, 2012, **5**, 6081-6088.

19. G. J. la O, S. J. Ahn, E. Crumlin, Y. Orikasa, M. D. Biegalski, H. M. Christen and Y. Shao-Horn, *Angew. Chem.-Int. Edit.*, 2010, **49**, 5344-5347.

20. J. Mizusaki, Y. Mima, S. Yamauchi, K. Fueki and H. Tagawa, *J. Solid State Chem.*, 1989, **80**, 102-111.

21. V. G. Sathe, A. V. Pimpale, V. Siruguri and S. K. Paranjpe, *Journal of Physics-Condensed Matter*, 1996, **8**, 3889-3896.

22. S. Y. Wang, J. Yoon, G. Kim, D. X. Huang, H. Y. Wang and A. J. Jacobson, *Chem. Mat.*, 2010, **22**, 776-782.

23. F. S. Baumann, J. Fleig, H. U. Habermeier and J. Maier, *Solid State Ion.*, 2006, **177**, 1071-1081.

24. A. Esquirol, N. P. Brandon, J. A. Kilner and M. Mogensen, *J. Electrochem. Soc.*, 2004, **151**, A1847-A1855.

25. L. W. Tai, M. M. Nasrallah, H. U. Anderson, D. M. Sparlin and S. R. Sehlin, *Solid State Ion.*, 1995, **76**, 259-271.

26. L. W. Tai, M. M. Nasrallah, H. U. Anderson, D. M. Sparlin and S. R. Sehlin, *Solid State Ion.*, 1995, **76**, 273-283.

27. A. V. Berenov, A. Atkinson, J. A. Kilner, E. Bucher and W. Sitte, *Solid State Ion.*, 2010, **181**, 819-826.

28. Y. M. Kim, S. I. Pyun, J. S. Kim and G. J. Lee, *J. Electrochem. Soc.*, 2007, **154**, B802-B809.

29. G. Amow, I. J. Davidson and S. J. Skinner, *Solid State Ion.*, 2006, **177**, 1205-1210.

30. G. Amow and S. J. Skinner, *J. Solid State Electrochem.*, 2006, **10**, 538-546.

31. M. Burriel, G. Garcia, J. Santiso, J. A. Kilner, J. C. C. Richard and S. J. Skinner, *J. Mater. Chem.*, 2008, **18**, 416-422.

32. R. Sayers and S. J. Skinner, *J. Mater. Chem.*, 2010, **21**, 414-419.

33. V. V. Kharton, A. V. Kovalevsky, M. Avdeev, E. V. Tsipis, M. V. Patrakeev, A. A. Yaremchenko, E. N. Naumovich and J. R. Frade, *Chem. Mat.*, 2007, **19**, 2027-2033.

34. T. Nakamura, K. Yashiro, K. Sato and J. Mizusaki, *Solid State Ion.*, 2010, **181**, 292-299.

35. J. M. Bassat, P. Odier, A. Villesuzanne, C. Marin and M. Pouchard, *Solid State Ion.*,

2004, **167**, 341-347.

36. S. J. Skinner and J. A. Kilner, *Ionics*, 1999, **5**, 171-174.

37. S. J. Skinner and J. A. Kilner, *Solid State Ion.*, 2000, **135**, 709-712.

38. A. Aguadero, M. J. Escudero, M. Perez, J. A. Alonso and L. Daza, *J. Fuel Cell Sci. Technol.*, 2007, **4**, 294-298.

39. E. Boehm, J. M. Bassat, P. Dordor, F. Mauvy, J. C. Grenier and P. Stevens, *Solid State Ion.*, 2005, **176**, 2717-2725.

40. S. Shinomori, M. Kawasaki and Y. Tokura, *Appl. Phys. Lett.*, 2002, **80**, 574-576.

41. A. Yamada, Y. Suzuki, K. Saka, M. Uehara, D. Mori, R. Kanno, T. Kiguchi, F. Mauvy and J. C. Grenier, *Adv. Mater.*, 2008, **20**, 4124-+.

42. D. Lee, A. Grimaud, E. J. Crumlin, K. Mezghani, M. A. Habib, Z. Feng, W. T. Hong, M. D. Biegalski, H. M. Christen and Y. Shao-Horn, *The Journal of Physical Chemistry C*, 2013, **117**, 18789-18795.

43. A. Demourgues, F. Weill, B. Darriet, A. Wattiaux, J. C. Grenier, P. Gravereau and M. Pouchard, *J. Solid State Chem.*, 1993, **106**, 317-329.

44. J. Rodriguezcarvajal, M. T. Fernandezdiaz and J. L. Martinez, *Journal of Physics-Condensed Matter*, 1991, **3**, 3215-3234.

45. J. Gopalakrishnan, G. Colsmann and B. Reuter, *J. Solid State Chem.*, 1977, **22**, 145-149.

46. Y. Takeda, R. Kanno, M. Sakano, O. Yamamoto, M. Takano, Y. Bando, H. Akinaga, K. Takita and J. B. Goodenough, *Mater. Res. Bull.*, 1990, **25**, 293-306.

47. H. J. M. Bouwmeester, H. Kruidhof and A. J. Burggraaf, *Solid State Ion.*, 1994, **72**, 185-194.

48. E. J. Crumlin, E. Mutoro, S. J. Ahn, G. J. la O, D. N. Leonard, A. Borisevich, M. D.

Biegalski, H. M. Christen and Y. Shao-Horn, *J. Phys. Chem. Lett.*, 2010, **1**, 3149-3155.

49. J. Maier, *Physical Chemistry of Ionic Materials: Ions and Electrons in Solids* John Wiley, Chichester, England ; Hoboken, NJ, 2004.

50. G. Kresse and J. Furthmuller, *Phys. Rev. B*, 1996, **54**, 11169-11186.

51. G. Kresse and J. Hafner, *Phys. Rev. B*, 1993, **47**, 558-561.

52. P. E. Blochl, *Phys. Rev. B*, 1994, **50**, 17953-17979.

53. J. P. Perdew and Y. Wang, *Phys. Rev. B*, 1992, **45**, 13244-13249.

54. V. I. Anisimov, F. Aryasetiawan and A. I. Lichtenstein, *Journal of Physics-Condensed Matter*, 1997, **9**, 767-808.

55. S. L. Dudarev, G. A. Botton, S. Y. Savrasov, C. J. Humphreys and A. P. Sutton, *Phys. Rev. B*, 1998, **57**, 1505-1509.

56. G. Kim, S. Wang, A. J. Jacobson and C. L. Chen, *Solid State Ion.*, 2006, **177**, 1461-1467.

57. M. S. D. Read, M. S. Islam, G. W. Watson and F. E. Hancock, *J. Mater. Chem.*, 2001, **11**, 2597-2602.

58. J. Maier, *Solid State Ion.*, 1998, **112**, 197-228.

59. V. V. Vashook, Yushkevich, II, L. V. Kokhanovsky, L. V. Makhnach, S. P. Tolochko, I. F. Kononyuk, H. Ullmann and H. Altenburg, *Solid State Ion.*, 1999, **119**, 23-30.

60. J. W. Han and B. Yildiz, *Energy Environ. Sci.*, 2012, **5**, 8598-8607.

61. F. Calle-Vallejo, N. G. Inoglu, H. Y. Su, J. I. Martinez, I. C. Man, M. T. M. Koper, J. R. Kitchin and J. Rossmeisl, *Chem. Sci.*, 2013, **4**, 1245-1249.

62. M. Burriel, J. Santiso, M. D. Rossell, G. Van Tendeloo, A. Figueras and G. Garcia, *J. Phys. Chem. C*, 2008, **112**, 10982-10987.

63. J. A. Kilner and C. K. M. Shaw, *Solid State Ion.*, 2002, **154**, 523-527.

Table of Content (max: 8cm x 4cm)

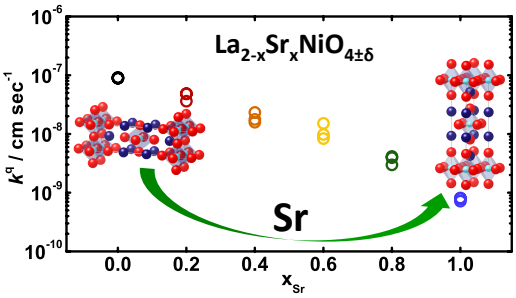

Strong Sr dependence of the oxygen surface exchange kinetics for the $La_{2-x}Sr_xNiO_{4\pm\delta}$ (LSNO) thin films

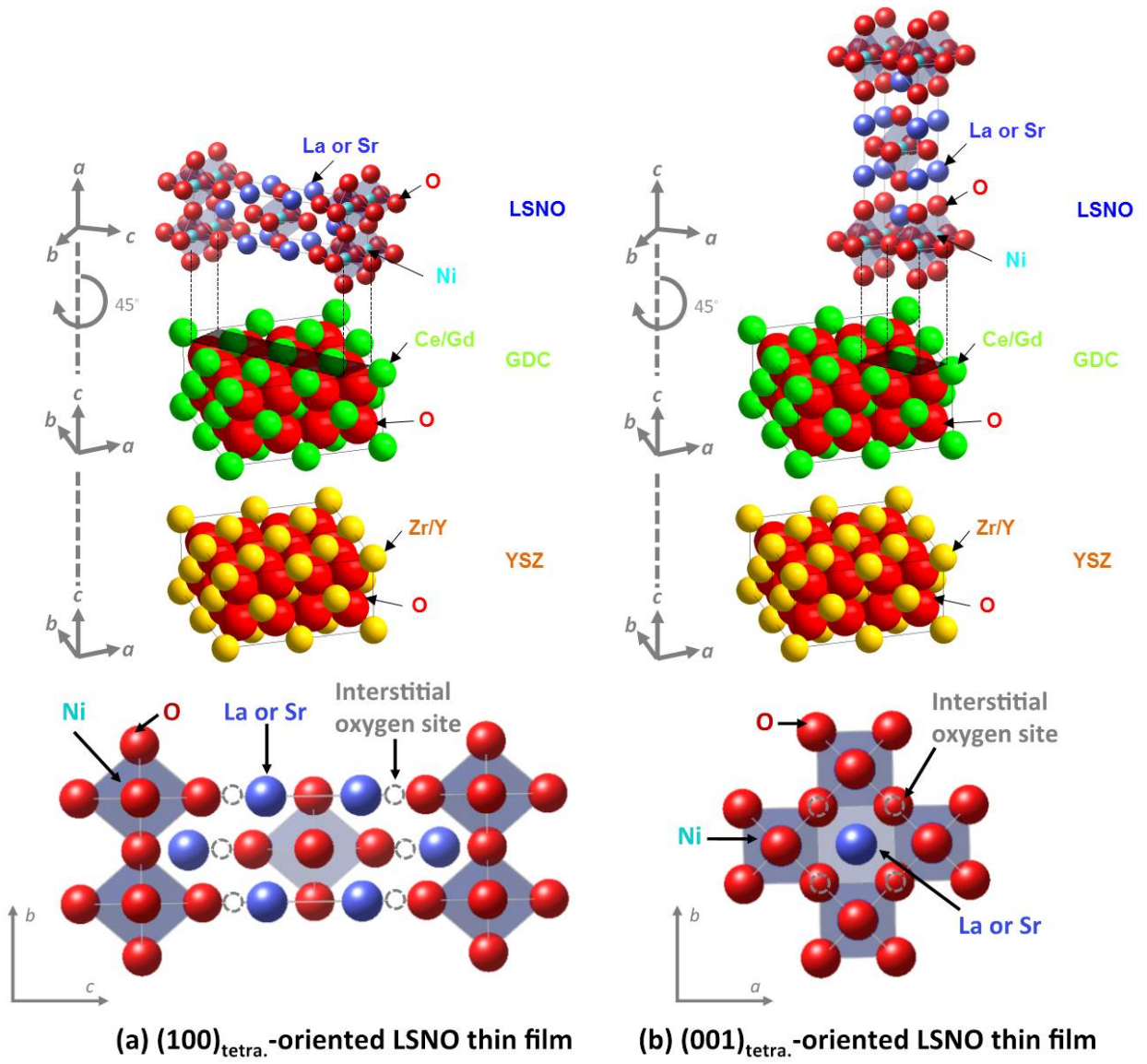

Fig. 1 Schematic of the crystallographic rotational relationships of LSNO $(l00)_{tetra.}$, GDC $(00l)_{cubic}$ and YSZ $(00l)_{cubic}$ ((a) top) and LSNO $(00l)_{tetra.}$, GDC $(00l)_{cubic}$ and YSZ $(00l)_{cubic}$ ((b) top). $(100)_{tetra.}$ top view of LSNO thin film ((a) bottom) and $(001)_{tetra.}$ top view of LSNO thin film ((b) bottom).

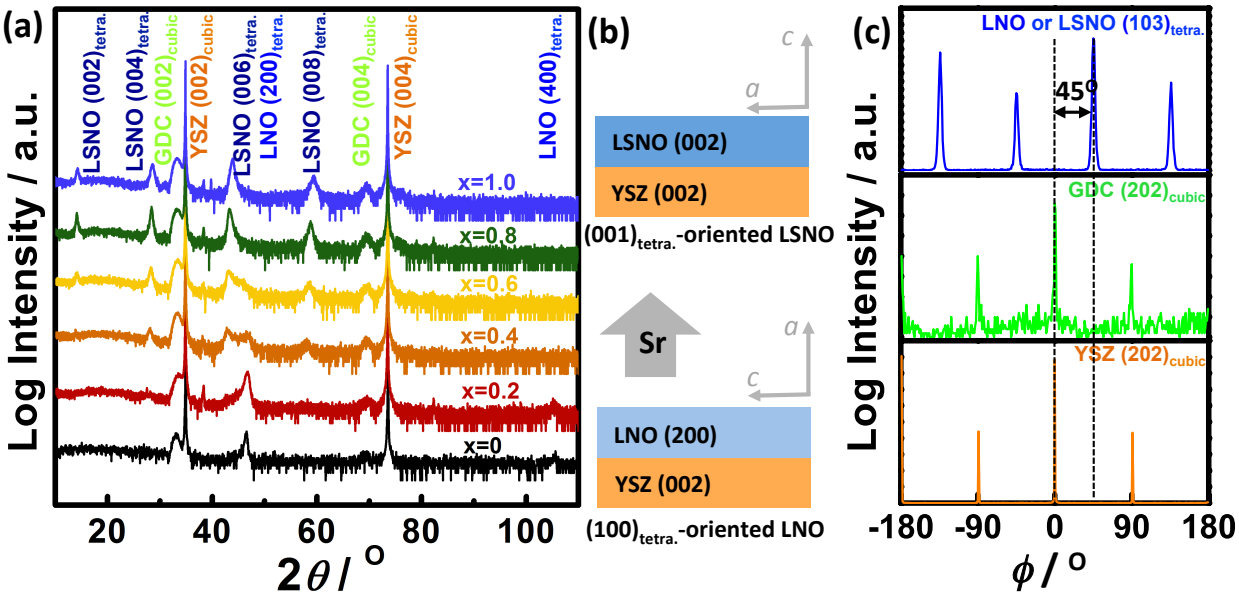

Fig. 2 HRXRD analysis (a) Normal XRD of the $La_{2-x}Sr_xNiO_{4\pm\delta}$ (LSNO) thin films with $0 \leq x_{Sr} \leq 1.0$, (b) schematic of a structural reorientation from $(100)_{tetra.}$ to $(001)_{tetra.}$ orientation with increasing Sr contents from LNO ($x_{Sr} = 0.0$) to LSNO ($x_{Sr} = 1.0$), and (c) Off-normal XRD of $\boldsymbol{a}_{tetra.}$-axis-oriented LNO $(103)_{tetra.}$ and $\boldsymbol{c}_{tetra.}$-axis-oriented LSNO $(103)_{tetragonal}$, GDC $(202)_{cubic}$, and YSZ$(202)_{cubic}$.

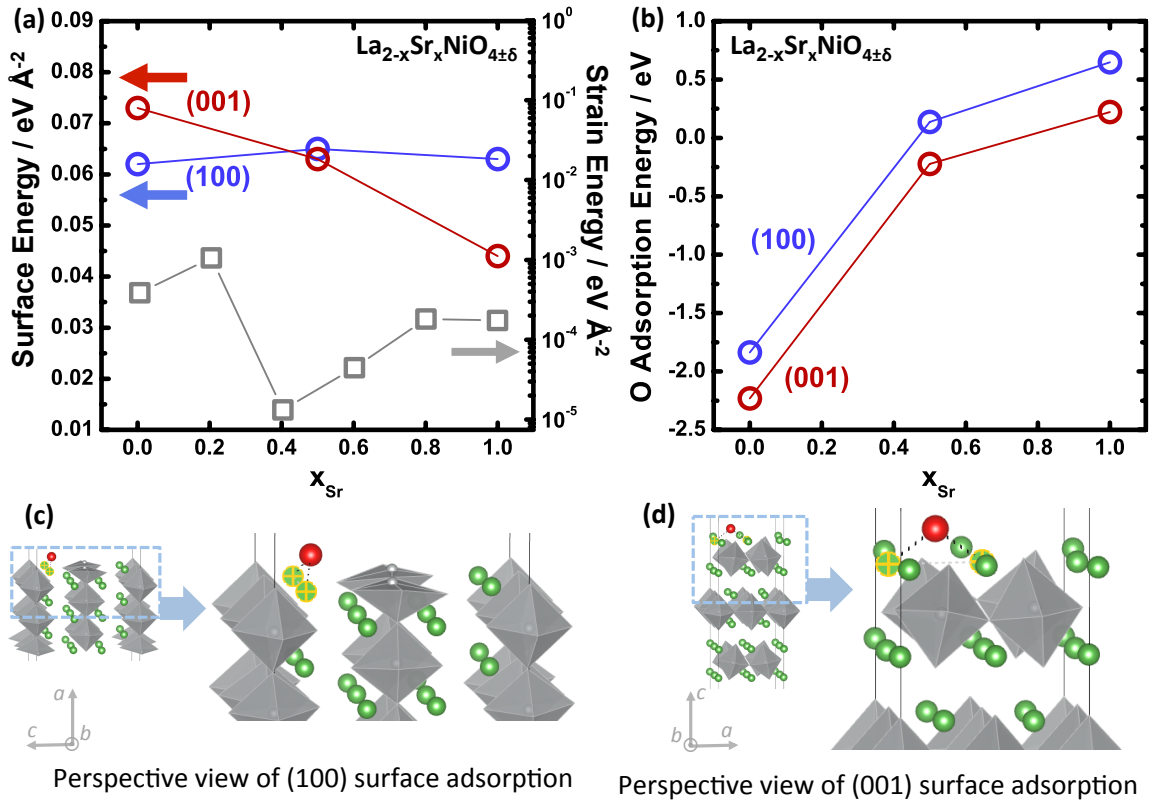

Fig. 3 Sr content dependency of (a) strain energies (□-gray) of the $La_{2-x}Sr_xNiO_{4\pm\delta}$ (LSNO) thin films with $0.0 \leq x_{Sr} \leq 1.0$ calculated using strain energy density equation, surface energies, and (b) adsorption energies of an oxygen molecule on the $(100)_{tetra.}$ (○-blue) and $(001)_{tetra.}$ (○-red) surfaces of the LSNO thin films calculated by density functional theory (DFT). The surface oxygen adsorption sites of (c) the $(100)_{tetra.}$ slabs and (d) the $(001)_{tetra.}$ slabs. Details of the DFT modeling approaches, the LSNO slab models, and strain energy calculation are provided in the ESI. Both surface energies and adsorption energies represent the anisotropic feature of the LSNO thin films.

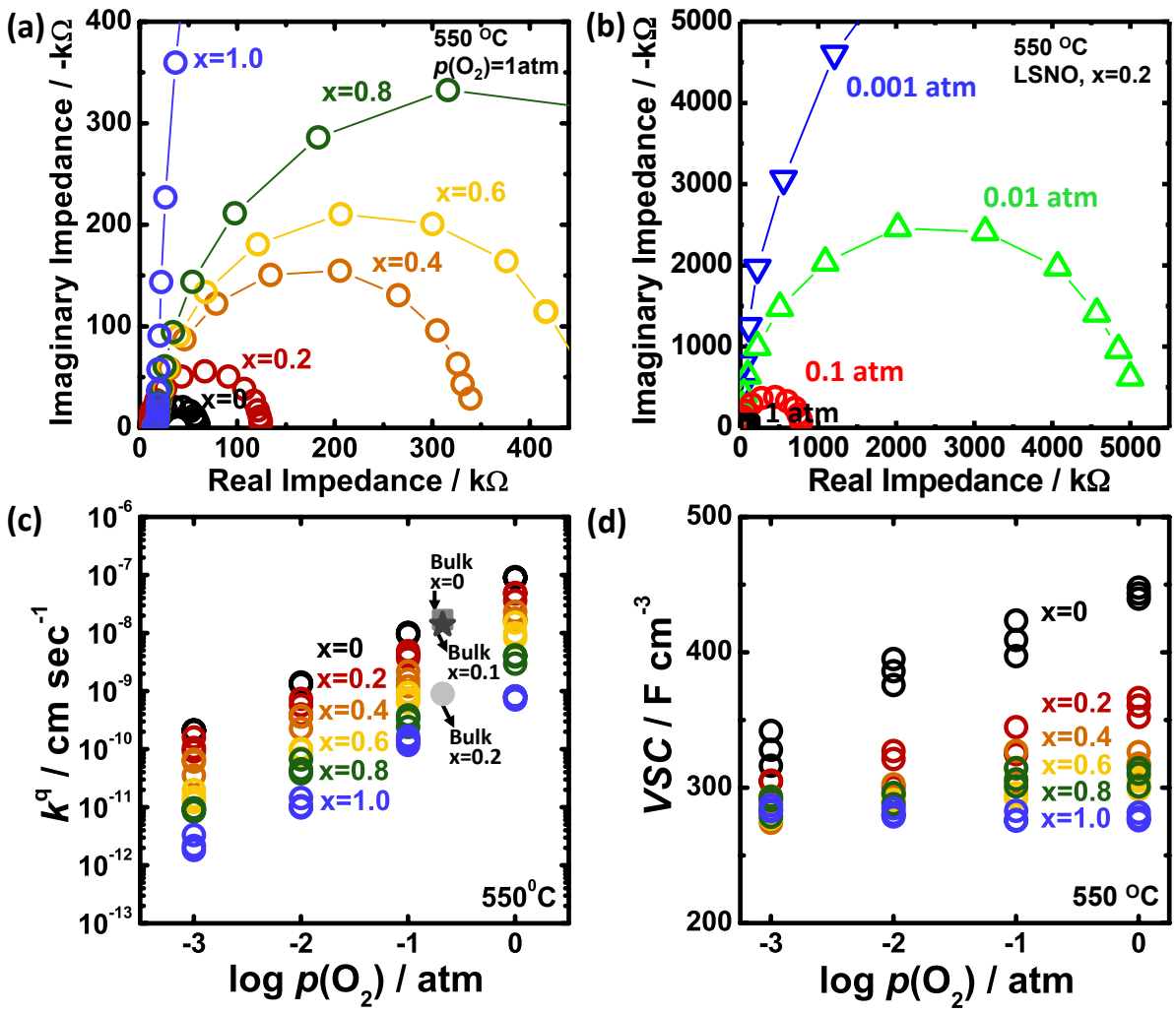

Fig. 4 Electrochemical impedance spectroscopy (EIS) results of microelectrodes for $La_{2-x}Sr_xNiO_{4\pm\delta}$ (LSNO) thin films with $0.0 \leq x_{Sr} \leq 1.0$ at 550 ^{O}C (a) Nyquist plot of the LSNO films in 1 atm. (b) Nyquist plot of the LSNO thin film with $x_{Sr} = 0.2$ as a function of $p(O_2)$. (c) Oxygen partial pressure dependency of the surface exchange coefficients of LSNO thin films calculated from EIS spectra collected at 550 ^{O}C. Extrapolated bulk k^* (approximately equivalent to k^q)[58] values obtained from previous data of (■-gray) Kilner et al.,[63] (★-dark gray) and (●-light gray) Boehm et al.,[39] are plotted for comparison. (d) Oxygen partial pressure dependency of volume specific capacitance (*VSC*) of LSNO thin films calculated from EIS spectra collected at 550 °C.

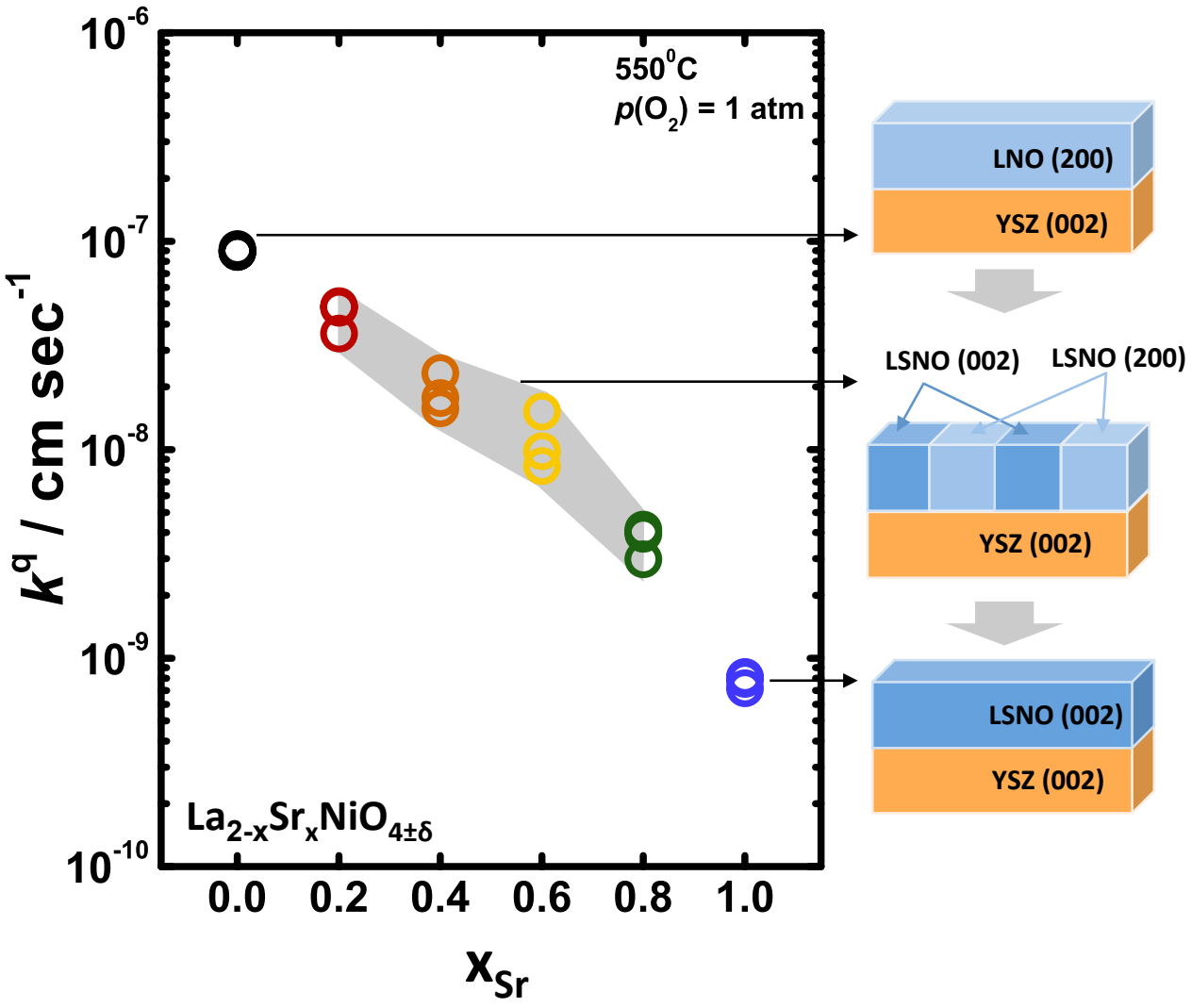

Fig. 5 Sr content dependency of the k^q of the $La_{2-x}Sr_xNiO_{4\pm\delta}$ (LSNO) thin films with $0.0 \leq x_{Sr} \leq 1.0$ calculated from EIS spectra collected at 550 ^{O}C in an oxygen partial pressure of 1 atm. The schematic of $\boldsymbol{a}_{tetra.}$-axis-oriented LNO thin film, both $\boldsymbol{a}_{tetra.}$-axis and $\boldsymbol{c}_{tetra.}$-axis orientation coexistence LSNO thin films, and $\boldsymbol{c}_{tetra.}$-axis-oriented LSNO thin film are shown besides the graph.

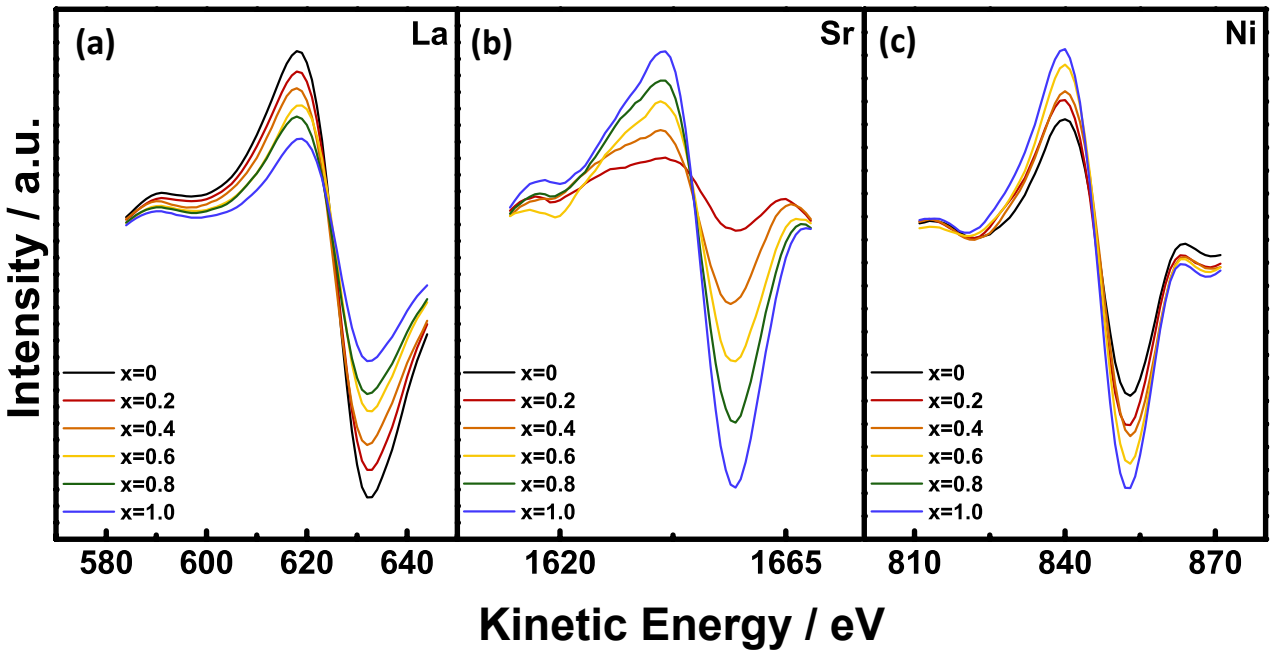

Fig. 6 Ex situ AES data of the $La_{2-x}Sr_xNiO_{4\pm\delta}$ (LSNO) thin films with $0.0 \leq x_{Sr} \leq 1.0$ annealed at 550 ºC in an oxygen partial pressure of 1 atm. (a) La_{MNN} cation variation (RSF: 0.059), (b) Sr_{LMM} cation variation (RSF: 0.027), and (c) Ni_{LMM} cation variation (RSF: 0.277) as a function of Sr contents. The change of La and Sr cation spectra scales with the La:Sr concentration and indicates that the surface chemistry is representative of the surface cationic ratio targeted. The change in the Ni cation spectra represents the change in the thin film orientation according to increase in NiO_6 octahedra population (normalized by surface area) with increasing the Sr content.